Microstructure Characterization of Oceanic Polyethylene Debris

Laura Rowenczyk, Alexandre Dazzi, Ariane Deniset-Besseau, Victoria Beltran, Dominique Goudounèche, Pascal Wong-Wah-Chung, Olivier Boyron, Matthieu George, Pascale Fabre, Clément Roux, et al.

Microstructure characterization of oceanic polyethylene debris

Laura Rowenczyk[1], Alexandre Dazzi[2], Ariane Deniset-Besseau[2], Victoria Beltran[3], Dominique Goudounèche[4], Pascal Wong-Wah-Chung[5], Olivier Boyron[6], Matthieu George[7], Pascale Fabre[7], Clément Roux[1], Anne Françoise Mingotaud[1] and Alexandra ter Halle[1]*

1. Laboratoire des IMRCP, Université de Toulouse, CNRS UMR 5623, Université Paul Sabatier, 118 route de Narbonne 31062 Toulouse Cedex 9, France
2. Laboratoire de Chimie Physique (LCP), CNRS UMR 8000, Univ. of Paris-Sud, Université Paris-Saclay, Orsay, France
3. IPANEMA, CNRS, Ministère de la Culture, UVSQ, USR3461, Université Paris-Saclay, F-91192 Gif-sur-Yvette, France
4. CMEAB, IFRBMT, Université de Toulouse, 133 route de Narbonne, Toulouse, France
5. Aix Marseille Univ, CNRS, LCE, Marseille, France
6. Université de Lyon, CPE Lyon, CNRS, UMR 5265, Laboratoire de Chimie Catalyse Polymères et Procédés (C2P2), Villeurbanne, France
7. Laboratoire Charles Coulomb (L2C), Univ Montpellier, CNRS, Montpellier, France.

*Corresponding author

KEYWORDS : polymer, nanoplastic, microplastic photodegradation, plastic weathering

ABSTRACT

Plastic pollution has become a worldwide concern. It was demonstrated that plastic breaks down to nanoscale particles in the environment, forming so-called nanoplastics. It is important to understand their ecological impact, but their structure is not elucidated. In this original work, we characterize the microstructure of oceanic polyethylene debris and compare them to the non-weathered objects. Cross-sections are analysed by several emergent mapping techniques. We highlight deep modifications of the debris within a layer a few hundred microns thick. The most

intense modifications are macromolecule oxidation and a considerable decrease in the molecular weight. The adsorption of organic pollutants and trace metals is also confined to this outer layer. Fragmentation of the oxidized layer of the plastic debris is the most likely source of nanoplastics. Consequently nanoplastic chemical nature differ greatly from plastics.

Introduction

The scientific community has defined plastic pollution as a major worldwide concern. Indeed, since the introduction of plastic in the 1950s, 6 300 million tons of plastic waste has been generated, a very large proportion of which has accumulated in landfills or the natural environment[1]. In addition to large microplastics (MPs, 1–5 mm), smaller plastic particles at the micrometre (µPs)[2-4] and nanometre (nanoplastics, NPs) scales[5-7] in the environment have been highlighted by recent studies. Because µPs and NPs exhibit very specific physico-chemical properties and reactivities, the evaluation of their potential toxicological impact require specific investigations[8]. Primary MPs and µPs are defined as particles purposely manufactured at this scale, such as beads, fibres and pellets[9]. Secondary MPs and µPs result from the breaking down or erosion of larger objects. These mechanisms already occur early in the life of the object[10]. Primary NPs is still very anecdotic because there is no manufacturing at large scale, NPs mainly result from the degradation of macroscopic plastic objects[6]. Under laboratory conditions, the erosion of MPs presenting an advanced stage of weathering favours the formation of NPs[11]. A major source of plastic pollution is the mismanagement of municipal waste[12], and fragmentation of these materials into micro- and nanosized particles is certainly a major degradation path[13].

Plastic degradation involves hydrolysis, mechanical abrasion, thermal degradation, biodegradation and/or photodegradation[10, 14, 15]. Commonly used plastics are mostly prone to photodegradation[16]. Plastic photodegradation leads to structural modification of the polymer

backbone, such as oxidation with the formation of carbonyl groups[17], chain scission, radical recombination and crosslinking[18]. Polymer photodegradation also leads to morphological alterations; the macromolecules can reorganize, and the crystallinity of the plastic often increases[19]. These physical transformations impact the mechanical properties of the material and favour breakdown and embrittlement[20]. Cracking, surface erosion and abrasion lead to the formation of µPs and NPs. Changes in the bulk properties of plastic in the ocean have been addressed[21-23], but the surface microstructure of plastic debris has not yet been thoroughly investigated.

The aim of this work is to provide new insights into modifications of the polymer microstructure upon weathering in the ocean and to elucidate the molecular structure of weathered plastics. Two oceanic plastic debris in polyethylene (PE) were selected because PE is the most commonly detected polymer in oceans[29,35]. The methodology of this study could be extended to investigate the microstructure of other weathered plastic such as polystyrene or polypropylene. The physico-chemical properties of the debris were compared to those of the original boxes, which allowed us to directly evaluate the impact of oceanic weathering. Cutting-edge technologies were deployed to precisely describe cross-sections and transverse sections of the material: micro-Fourier transform infrared (µFTIR) spectroscopy, infrared spectroscopy coupled to atomic force microscopy (nano-AFMIR) to measure the material oxidation, fluorescence microscopy to monitor the adsorption of organic compounds and scanning/transmission electron microscopies coupled with energy dispersive X-ray spectroscopy (EDS-SEM/TEM) to monitor the adsorption of inorganic compounds. As µPs and NPs are generated from weathered macroscopic plastic debris, this study provides essential information for the comprehension of the physico-chemical nature of µPs and NPs.

Materials and methods

Sample collection

Plastic debris was collected by boat in the North Atlantic sub-tropical gyre in June 2015 during the French *7th* Continent Expedition sea campaign[21]. Two of eight plastic debris samples of PE were selected here for the microstructure investigation. We selected a box of coffee and a box of cocoa powder and purchased new boxes for comparison (Figure SI 1).

Surface and bulk characterization

Characterizations by ATR-FTIR and measurements by DSC and SEC results were published in ter Halle et al. The PAH contents are presented in Bouhroum et al.[24], and the metal levels are reported in Prunier et al[25].

Fourier transform infrared (FTIR) spectroscopies

The µ-FTIR mappings were obtained in transmission mode using a Hyperion 3000 (BRUKER) equipped with a focal plan array (FPA) detector. Background and sample spectra were acquired using 256 scans at a spectral resolution of 4 cm^{-1}. Ten-micrometre-thick cross-sections were sealed in KBr pellets prior to observations. OPUS software allowed the CI maps to be drawn with the integration of the carbonyl absorption bands in the 1780-1660 cm^{-1} region and the methylene absorption band in the 1490 to 1420 cm^{-1} region. Spectra with high spectral and spatial resolution were obtained by AFMIR using a spectroscope. The spectra were generated with Analysis Studio software without any correction.

AFM characterization

Small-scale surface topographies were acquired by AFM using a Nanoscope V (Bruker) in contact mode.

Cross-section preparations

Cross-sections of the plastic samples were cut using a microtome with a diamond blade. Different thicknesses were obtained depending on the characterization technique. Cross-sections of 10 µm were used for the µ-FTIR and light and fluorescence microscopies. EDS-TEM required a thinner cut, and cross-sections of 150 nm were made specifically for this analysis. For AFMIR, the surface of the section was basically flattened using the microtome, and the measurements were performed directly on the plastic section. For EDS-MEB, the section was obtained by cryofracture.

Light and fluorescence microscopic observations

Light and fluorescence microscopies were performed using a digital slide imager NanoZoomer 2.0R.S (HAMAMATSU) equipped with an LX2000 200 W Ultrahigh-pressure mercury lamp. Observations were made at different excitation/emission wavelengths ($\lambda_{em}/\lambda_{ex}$): 359/461 nm, 495/519 nm, 552/578 nm 554/566 and 649/666 nm. The images were corrected with NDP view software to obtain a gain of 1.8 for the fluorescence observation.

EDS-SEM and EDS-TEM

TEM and scanning transmission electron microscopy (STEM) studies were performed using a JEOL cold-FEG JEM-ARM200F operated at 200 kV equipped with a probe Cs corrector reaching a spatial resolution of 0.078 nm. EDX spectra were recorded on a JEOL CENTURIO SDD detector.

Results and discussion

Mesoplastics were collected in the North Atlantic sub-tropical gyre during the 7th Continent Expedition. Two debris were easily identified as cocoa and coffee powder packaging items

named M_1 and M_2, respectively (Figure SI1). They were compared to two non-weathered original items (named I_1 and I_2, respectively). Most observations obtained for one pair of items (new and weathered) followed the same trend as those obtained for the other pair. Therefore, for clarity, we discuss the results for M_2 and I_2 in the text, and M_1 and I_1 data are presented in the Supplementary Information files.

Characterization of plastic bulks and surfaces

Table 1 summarizes the bulk and surface characteristics. For bulk characterization, we observed no significant alteration of the melting points and crystallinity between the mesoplastics and the original items. Polymer chain length is described by the number average molar mass (M_n) and the weight average molar mass (M_w), which can be measured by size exclusion chromatography (SEC). The M_n and M_w values were both significantly smaller for M_2 compared to I_2 : the M_n value was reduced by a factor 2.

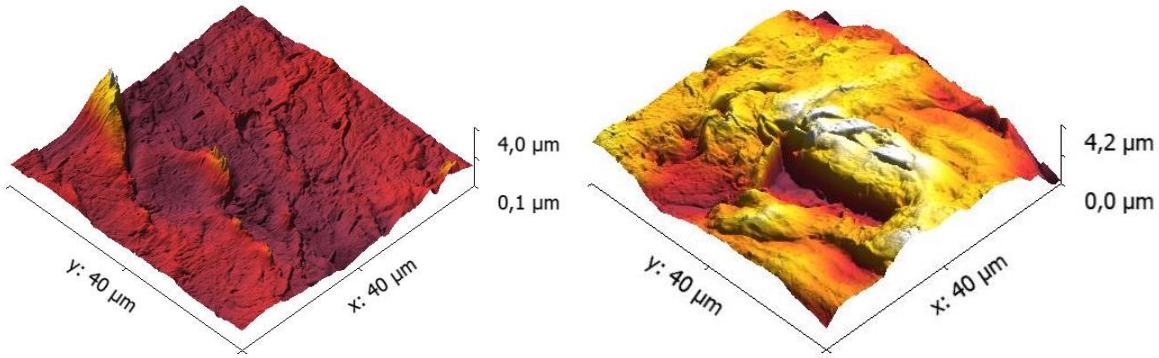

Figure 1: AFM characterization of the new coffee box (I_2) and the corresponding weathered object (M_2). The root mean square roughness values for the original box and the weathered object were 323 nm and 623 nm, respectively.

For surface characterization, the mesoplastics presented a significantly higher carbonyl index than the non-weathered item. Characterization of the plastic surface by atomic force microscopy

136 (AFM) shows that there is a significant increase in the root mean square (RMS) roughness by
137 at least a factor 2 (on 40x40 μm^2 areas, Figure 1 and Figure SI2). This roughening is induced
138 by the appearance of micro-sized peaks at a scale that is typical of semi-crystalline
139 arrangement[26]. We also observe that the thickness of the mesoplastic is lower than that of the
140 original box (reduction of 15 to 20%, Figure 2 and 4). A reduction in material thickness during
141 production to safe material resources may explain the difference in thickness but it can also be
142 envisaged that this thickness reduction is due to erosion; as it is observed upon polymer
143 photodegradation under controlled conditions[27].

144 The total level of polycyclic aromatic hydrocarbons (ΣPAHs) in the plastic samples were below
145 the detection limit for original items (Table 1), whereas mesoplastics contained measurable
146 levels of ΣPAHs in the range of ng/g. This finding is consistent with literature data[28]. The level
147 in M_2 was seven times higher than that in M_1. The important variations between ΣPAH levels
148 in plastic debris sampled in the same location have previously been noted[29].

149 For metal concentrations, the focus was made on four metals found in noticeable amounts: Fe,
150 Pb, Ti and Cr. A detailed analysis of metal concentrations in the sample collected during this
151 campaign is given elsewhere[25]. The presence of metals in the original items is because some
152 metals are incorporated during the manufacturing process (such as Ti and Fe) to improve plastic
153 properties. All metal concentrations were systematically higher in the mesoplastics than in the
154 original items because of sorption phenomena. The most explicit results were observed for Pb
155 and Cr, as their quantities were 55 000 and 1 100 times higher in M_1 than in I_1, respectively.
156 Large variability from one sample to another was also observed[30], and this variability is difficult
157 to rationalize.

158 Table 1: Characterizations of bulk material by [a)] attenuated total reflectance FTIR, [b)] calorimetry

(DSC), and [c] SEC; [d] total level of polycyclic aromatic hydrocarbons measured by HPLC-FLD (sum of eight PAH levels); and [e] metal concentrations determined by ICP-MS

		I_1	M_1	I_2	M_2
MATERIAL PARAMETERS	**Carbonyl Index**[a]	0.1	0.7	0	0.3
	Melting point[b] **Endset** (°C)	141.8	135.7	142	142.7
	Crystallinity[b] (%)	41	39	43	42
	M_n [c] ($kg\ mol^{-1}$)	21.0	10.9	12.3	7.1
	M_w [c] ($kg\ mol^{-1}$)	85.5	80.8	94.0	67.5
PAH/METAL CONCENTRATIONS	**ΣPAHs** [d] ($ng\ g^{-1}$)	ND	2.2	ND	15.3
	Fe ($\mu g\ g^{-1}$)	1.1	19.2	ND	58.1*
	Pb ($\mu g\ g^{-1}$)	0.05	2760.45	ND	0.02*
	Ti ($\mu g\ g^{-1}$)	42.5	78.5	ND	8.8*
	Cr ($\mu g\ g^{-1}$)	0.8	866.2	ND	3.0*

*Average of two values.

To summarize, surface characterization were more sensitive than bulk characterization to highlights some structural modifications of the polymer upon weathering. While calorimetry does not allow us to measure differences in the melting point or the percentage of crystallinity, the molar masses (M_n and M_w) was more sensitive parameters. Both metals and organic pollutants can be sorbed by plastic debris in large amounts.

Oxidation profile

For the microstructure investigation, cross-sections were obtained using different methods to

produce samples with thicknesses adapted to each characterization technique (Figure SI 3). µ-FTIR mapping of the cross-sections allowed us to obtain a cartography of the carbonyl index (Figure 2). The coffee box sample I_2 exhibited a low and uniform carbonyl index across the whole cross-section (upper mapping in Figure 2). I_2 is not oxidized on its surfaces or at its centre. In contrast, cross-section mapping of M_2 highlights a highly oxidized external face, with a deep oxidation gradient from the edge towards the centre. Oxidation was observed at depths of up to 500-600 µm within the material; one can note that the oxidation layer is heterogeneous at the micrometre scale. The internal face appeared much less oxidized. The rate of oxygen diffusion into the material presumably evolves with the material aging. With aging the surface becomes more porous and could facilitate oxygen transport and further deep oxidation of the debris.

AFMIR is a recently developed cutting-edge technique that combines the high spatial resolution of an AFM and the chemical characterization offered by IR spectroscopy[31]. AFMIR presents a high spatial resolution of ten nanometres. Spectra were acquired between 900 or 1350 cm-1 and 1900 cm-1. Punctual measurements (30 x 30 nm) were performed at three different locations along the cross-section (external and internal faces and centre).

The AFMIR spectra of M_2 (Figure 2 A and SI4) indicated that the oxidation band was more intense and broader than that of I_2 and was shifted to 1712 cm^{-1}. The broadening of the oxidation band is explained by the presence of various oxidation products. As frequently reported in the literature, photooxidation of PE generates ketones (peak at 1720 cm^{-1}) in the initial step. In addition, secondary processes lead to the formation of carboxylic acids (1713 cm^{-1}), esters (1735 cm^{-1}) and lactones (1780 cm^{-1})[32]. The absorption band at 1641 cm^{-1} is attributed to the formation of double bonds during PE photodegradation. Both the oxidation and double bound bands were detected in the three scanned regions of the macrodebris. Thus, even within the

194 material, the products of photodegradation are detected. This finding is in agreement with the
195 μFTIR mapping that indicated a deep oxidation gradient from the edge towards the centre of
196 the material section. Those local IR absorption spectra also gives an information about the
197 crystallinity of the sample. The relative intensity of the 1473-1464 cm^{-1} peak may vary from
198 point to another. This might be an orientation effect generated during item production.
199 Furthermore, M_2 shows a shoulder at 1438 cm^{-1} and several weak absorption bands at 1370-
200 1354 and 1303 cm^{-1}. Generally, in pure crystalline product, 1354 and 1303 cm^{-1} (also called
201 amorphous bands[33]) weak bands are absent[34] and the wagging mode of CH_2 at 1370 cm^{-1} is
202 more intense. Figure 2 B. shows the IR response of crystalline hentriacontane for whom the
203 intensity the wagging mode at 1370 cm^{-1} is largely higher than the two other bands (1354 and
204 1303 cm^{-1}). When comparing the AFMIR spectra of M2 internal and external face we cannot
205 establish if one face is more crystalline than another.

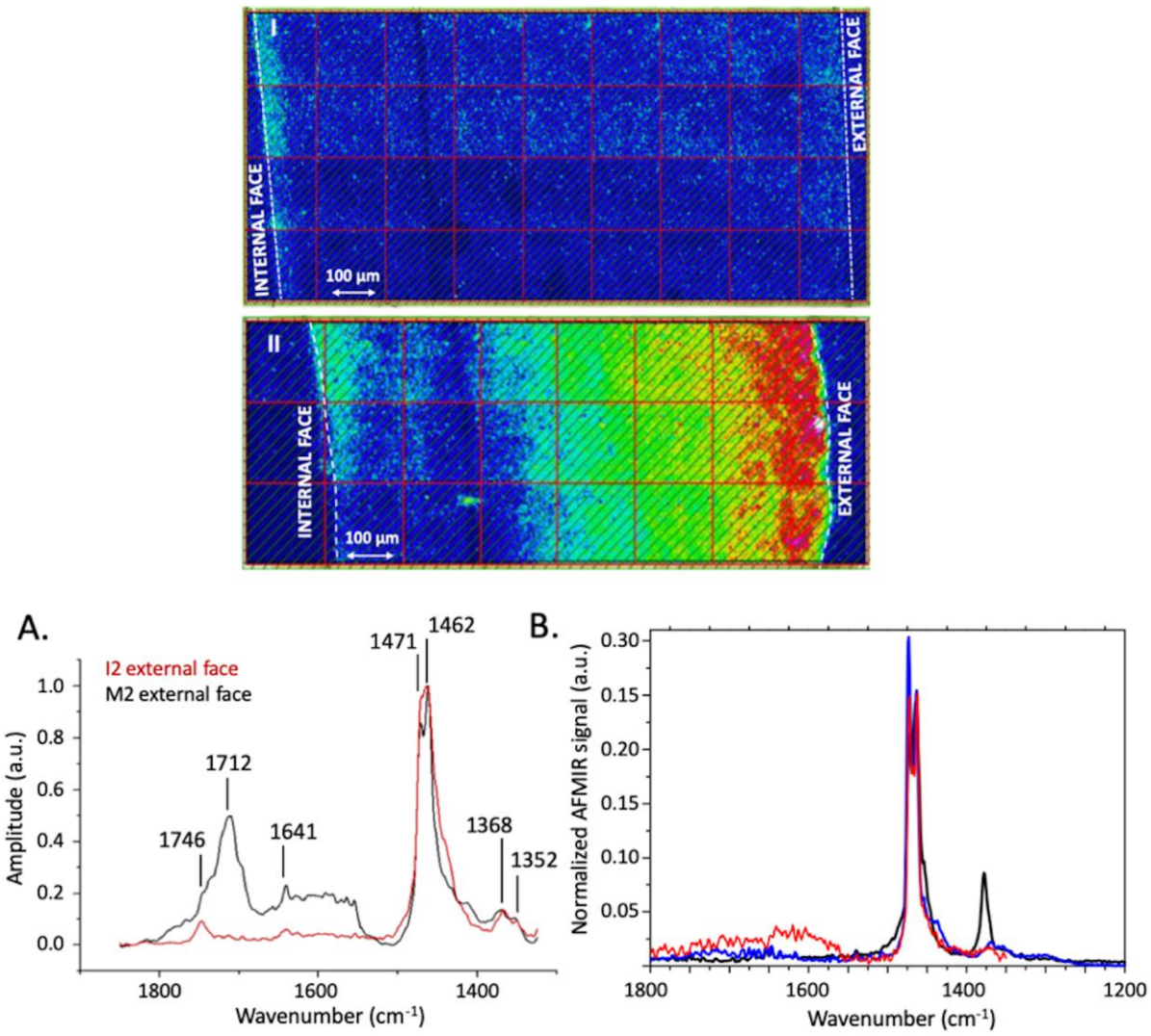

206

207 Figure 2: On the top: profile of oxidation obtained by µ-FTIR with a representation of the
208 carbonyl index mapping of the new coffee box I_2 (I) and the mesoplastic M_2 (II). At the bottom :
209 A) local AFMIR spectra at the external face of the original coffee box (black) and the
210 mesoplastic (red) B) local AFMIR spectra of hentriacontane (black), internal face of the
211 mesoplastic (blue) and external face (red). The internal face appears less oxidized than the
212 external face.

213 **Calorimetric characterization of the transverse section**

214 For the microstructure investigation, the materials were sectioned transversally with a thickness

of 100 µm for DSC analysis (Supplementary Table 1). Bulk DSC measurements did not highlight differences between the original items and the mesoplastics. While I_2 edges were only slightly more crystalline than the core material (1 to 2% ±1%). The heterogeneity of I_2 may be a result of the manufacturing process (during injection moulding) or may be because the box was exposed to light and already underwent slight photodegradation during storage. On the contrary M_2 external face was significantly different from the core material, while the internal face presented fewer differences (Figure 3). The degree of crystallinity of the external face increased by 6% compared to that of the core material, and the melting point decreased by 3°C. The increase in crystallinity of plastics debris is explained by two parameters[21]. First explanation is that amorphous regions are more easily degraded. The second is that polymer degradation increases the mobility of the macromolecules, which can form new crystals. Due to degradation, the molar mass of the chains is decreased, and therefore, the lamellae of the folded chain are shorter. The shorter macromolecules are more mobile and this allow them to crystalize[35]. Consequently weathered polyethylene are more crystalline than pristine. The resultant crystals obtained with a shorter folding length are smaller than the original crystals; therefore, they exhibit a lower melting point (the lower the folding length is, the lower the corresponding melting point)[36-38]. The observed lower melting point of the resulting materiel indicates that the new crystals are of a lesser quality compare to the pristine ones. This can be linked either to the lower molecular weight of the polymer chains involved or to a very slow crystallization process. Since it is not possible to evaluate the aging time of the samples, we cannot discriminate between these two posisbilities. We also noticed a significant narrowing of the melting curves for the external faces compared to the rest of the material (Figure SI 5 and 6).

SEC of the transverse section

The transverse sections were analysed by SEC (details in Supplementary Table 1). Generally speaking, polymer photodegradation has a greater effect on the longer macromolecular chains, and M_w is more sensitive than M_n to polymer chain scission. Mw data is presented here and Mn in supplementary material (Table SI 1). I_2 presented an inhomogeneity in the molar mass, but the variations in M_2 were much greater. Again, the external face of the mesoplastics presented the most intense modifications (Figure 3) with a M_w value decreased by 80%. M_2 external face presents a molecular weight of only 20 000 g/mol.

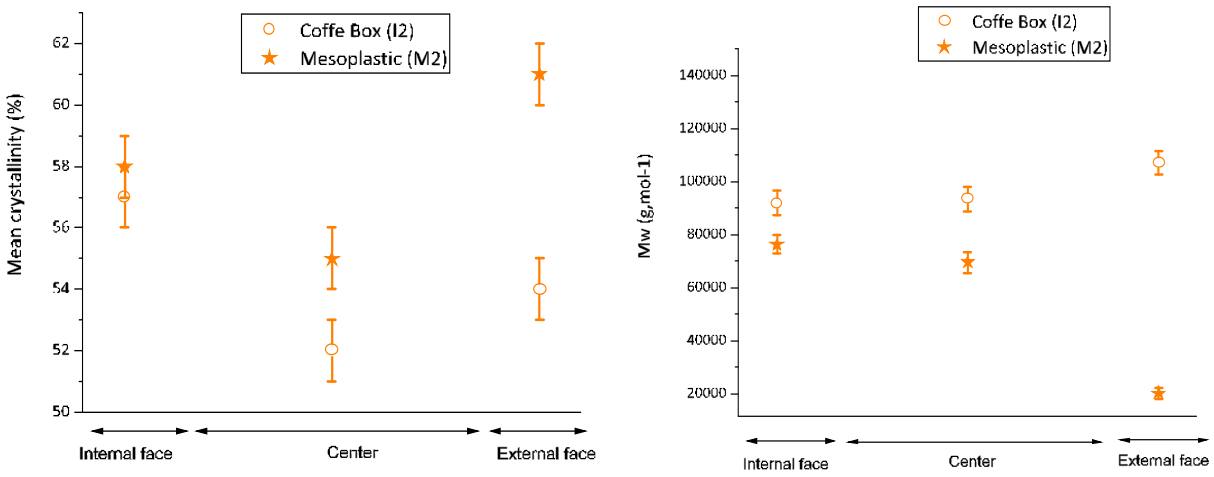

Figure 3: On the left, percentage of crystallinity and on the right weight average molar mass (M_w). Data measured for the transverse sections (internal and external with a thickness of 100 µm) and the core material (thickness of 1 mm).

Fluorescence and electronic microscopy of cross-sections

When excited, I_2 emitted an intense fluorescence, particularly at an excitation wavelength of 554 nm (Figure 4). The initial fluorescence of I_2 is attributed to additives, probably dyes of the quinacridone family[39]. The fluorescence emitted by M_2 at this excitation wavelength was much less intense, which may be because a result of the additive either migrating out of the materials[40] or being degraded[41]. Although typical results for plastic additive desorption under normal

255 conditions of use are generally known[42, 43], the desorption of additives under weathering
256 conditions has been less described.

257 At 359 nm, although I_1 and I_2 were not fluorescent M_1 and M_2 (Figure 4 and SI 7) exhibited a
258 fluorescence gradient from the external face towards the centre in the range of 200 to 400 µm.
259 This fluorescence indicates the presence of new aromatic compounds in the material and could
260 be attributed to PAHs that present characteristic fluorescence[44-46] with an excitation wavelength
261 between 255 and 365 nm. This signal could also be attributed to marine dissolved organic
262 matter[47] or the products of degradation of additives within the plastic. It is important to note
263 that these fluorescent chemicals are sorbed within the first hundred microns of the materials
264 and could easily leach, for example, in the case of ingestion, where the pH conditions could
265 favour transfer to the organisms.

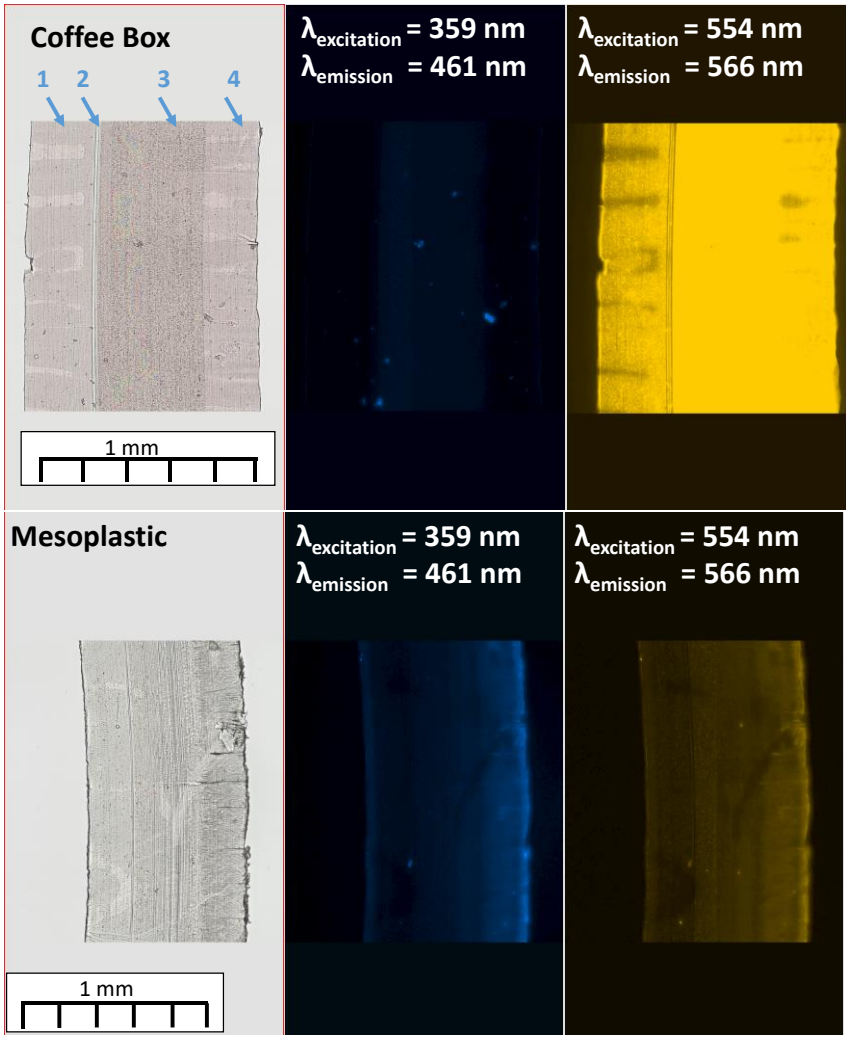

Figure 4: Microscopic observations of the new item (I_2) and the mesoplastic (M_2). On the left is a bright field image, and on the right are fluorescence images.

The atomic composition of the cross-sections was characterized by EDS-TEM. Numerous Ca and Ti ion-based particles were found in all four materials (Figure SI 8 to 10). Particles containing calcium were between 5 and 10 µm, and Ti ion-based particles were larger (200 to 500 nm). Inorganic compounds are included in the plastic formulation as additives to improve some of the material properties like $CaCO_3$ particles that are used as plastic fillers. These particles were randomly distributed in the carbon matrix and were also found in the mesoplastics, so there is no evidence for their leaching upon weathering. Some deep cracks

were observed, filled with sea salt crystals (Figure 5c and SI 11) Numerous nanoparticles were detected on M_2 external face (Figure 5a). The nanoparticles contained high amounts of Fe. Iron was systematically present with Mn, Ni and Zn (Figure SI 12 and 13). These observations confirm the occurrence of a recently described process[25]: the formation of Fe or Mn precipitated minerals on plastic debris surfaces in the ocean. It was also demonstrated that polymer oxidation promotes metal sorption[25]. It is noticeable to mention that high amounts of Pb was detected in bulk M_1 and EDS-TEM revealed the presence of elongated Pb particles with a size between 100 and 200 nm (Figure SI 14 and 15).

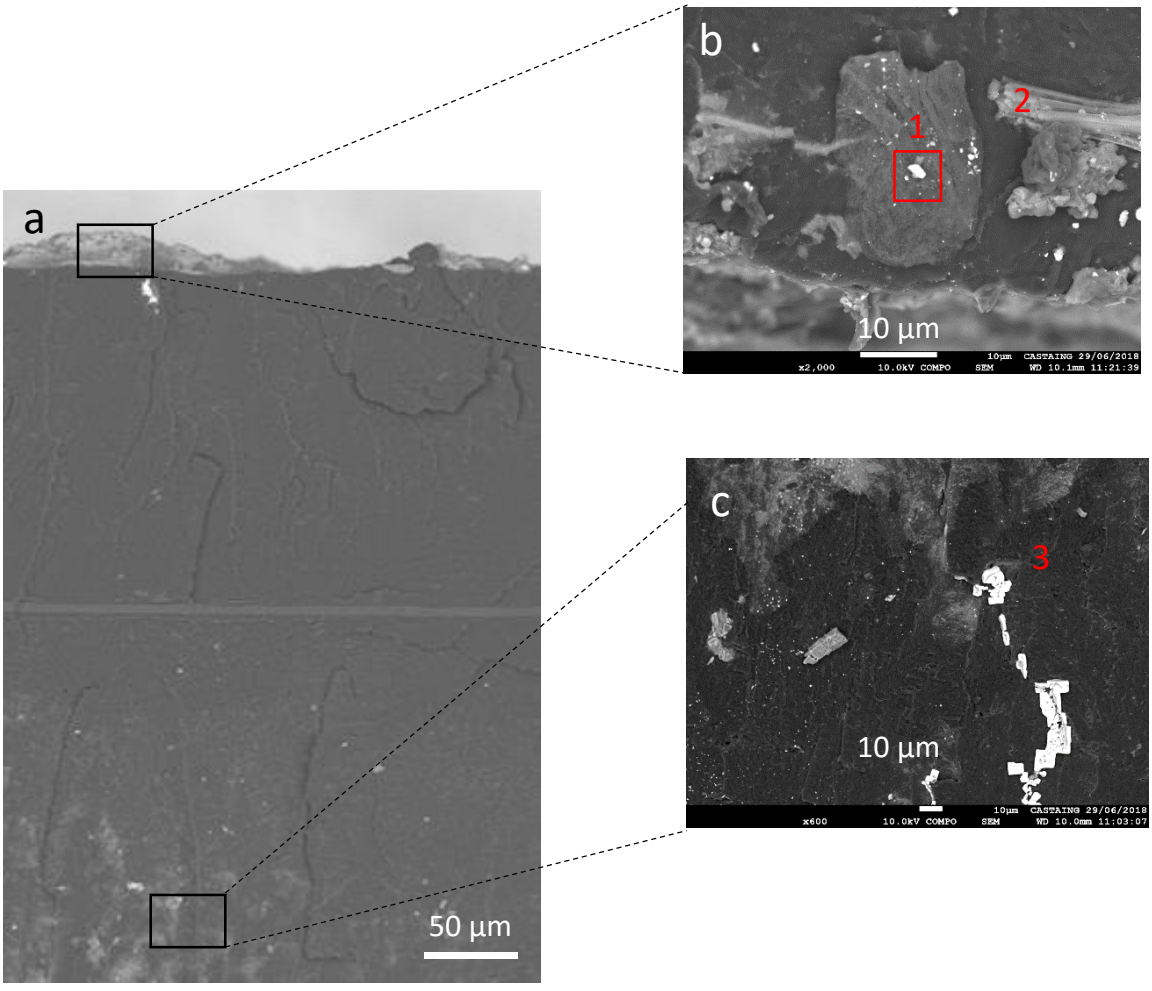

Figure 5: EDS-SEM observations of M_2. a: view of the whole transverse section, b: magnification of a part of the external face, c: magnification of deep cracks filled with sea salt

crystals. The multilayer structure of the polymer is elucidated by EDX-SEM (Figure SI 16) and is composed of ethylene vinyl alcohol copolymer.

As a conclusion, the microstructure investigation of ocean-weathered mesoplastics compared to original items has highlighted strong morphological, structural and molecular modifications of the outer layer of the material. We also could observe that the outer side was more altered certainly because more exposed to UV. Whereas bulk characterization did not allow to detect deep modifications. The microstructure investigation showed that the outer layers of the debris were remarkably more crystalline than the rest of the material. This outer layer consisted also of very shorten and highly oxidized polyethylene macromolecules. All these modifications are expected to eventually affect the mechanical properties of the polymer and lead to embrittlement[48-50]. Embrittlement, fragmentation and delamination of the affected surface layer are most likely linked with the non-homogeneous erosion of the surface layer, leading to a strong increase in the surface roughness. The spatial distributions of oxidation and roughening are on the same scale as the polymer semi-crystalline microstructure (micrometre). This process mainly involves fragmentation into µPs and NPs, which explains the significant thickness decrease of the mesoplastics. The generation of NPs from microplastics was observed by Gigault et al.[11]. This study also demonstrated the strong sorption of organic and inorganic chemicals, mostly localized on the outer layer. The field of NP investigation is new, and there is no description of the molecular structure of nanoplastics. What are NPs are made of? How are the macromolecules organized in NPs? As µPs and NPs result from fragmentation of the outer layer of macrodebris, their structure is certainly similar to that of the outer layer. The present study provides insight into the structure of µPs and NPs. We conclude that µPs and NPs are certainly composed of macromolecules that differ greatly from those composing plastics; these macromolecules are highly oxidized and significantly shorter. We also conclude that NPs

interact with species like trace metals or organic compounds originating from sorption on plastic debris surfaces. Overall, NP structural investigations must be conducted, or it will not be possible to understand their fate in oceans or their potential impact on ecosystem and human health.

ASSOCIATED CONTENT

Supporting Information Additional experimental details, including a photo of the macrodebris and the GPS coordinates were they have been collected. The characterization of M_1 and I_1 by AFM, AFMIR, calorimetry, GPC and fluorescence microscopy. Additional SEM, EDX-SEM and EDX-TEM data are also presented in the Supplementary Information in Figure SI 1 to 15 and Table SI 1

Funding Sources

This project is supported by the Total Corporate Foundation Foundation and The French National Reaserch Program for Environmental and Occupational Health of Anses (EST/2017/1/219).

ACKNOWLEDGEMENT

We thank the 7th Continent Expedition association, as well as the staff and crew, for the sea sampling campaign.

REFERENCES

1. Geyer, R.; Jambeck, J.; Lavender Law, K. Production, use, and fate of all plastics ever made. *Science Advances* **2017,** (7).
2. Andrady, A. L. Microplastics in the marine environment. *Mar Pollut Bull* **2011,** *62* (8), 1596-1605.
3. Song, Y. K.; Hong, S. H.; Jang, M.; Kang, J. H.; Kwon, O. Y.; Han, G. M.; Shim, W. J. Large Accumulation of Micro-sized Synthetic Polymer Particles in the Sea Surface Microlayer. *Environ Sci Technol* **2014,** *48* (16), 9014-9021.
4. Thompson, R. C.; Olsen, Y.; Mitchell, R. P.; Davis, A.; Rowland, S. J.; John, A. W. G.;

McGonigle, D.; Russell, A. E. Lost at sea: Where is all the plastic? *Science* **2004,** *304* (5672), 838-838.
5. Ter Halle, A.; Jeanneau, L.; Martignac, M.; Jarde, E.; Pedrono, B.; Brach, L.; Gigault, J. Nanoplastic in the North Atlantic Subtropical Gyre. *Environ Sci Technol* **2017,** *51* (23), 13689-13697.
6. Gigault, J.; ter Halle, A.; Baudrimont, M.; Pascal, P. Y.; Gauffre, F.; Phi, T. L.; El Hadri, H.; Grassl, B.; Reynaud, S. Current opinion: What is a nanoplastic? *Environ Pollut* **2018,** *235*, 1030-1034.
7. Mintenig, S. M.; Bauerlein, P. S.; Koelmans, A. A.; Dekker, S. C.; van Wezel, A. P. Closing the gap between small and smaller: towards a framework to analyse nano- and microplastics in aqueous environmental samples. *Environmental Science-Nano* **2018,** *5* (7), 1640-1649.
8. Galloway, T. S.; Cole, M.; Lewis, C. Interactions of microplastic debris throughout the marine ecosystem. *Nature Ecology & Evolution* **2017,** *1* (5).
9. Rochman, C. M.; Kross, S. M.; Armstrong, J. B.; Bogan, M. T.; Darling, E. S.; Green, S. J.; Smyth, A. R.; Verissimo, D. Scientific Evidence Supports a Ban on Microbeads (vol 49, pg 10759, 2015). *Environ. Sci. Technol.* **2015,** *49* (24), 14740-14740.
10. Lambert, S.; Wagner, M. Characterisation of nanoplastics during the degradation of polystyrene. *Chemosphere* **2016,** *145*, 265-268.
11. Gigault, J.; Pedrono, B.; Maxit, B.; Ter Halle, A. Marine plastic litter: the unanalyzed nano-fraction. *Environmental Science-Nano* **2016,** *3* (2), 346-350.
12. Jambeck, J. R.; Geyer, R.; Wilcox, C.; Siegler, T. R.; Perryman, M.; Andrady, A.; Narayan, R.; Law, K. L. Plastic waste inputs from land into the ocean. *Science* **2015,** *347* (6223), 768-771.
13. Bouwmeester, H.; Hollman, P. C. H.; Peters, R. J. B. Potential Health Impact of Environmentally Released Micro- and Nanoplastics in the Human Food Production Chain: Experiences from Nanotoxicology. *Environ Sci Technol* **2015,** *49* (15), 8932-8947.
14. ter Halle, A.; Ladirat, L.; Gendre, X.; Goudouneche, D.; Pusineri, C.; Routaboul, C.; Tenailleau, C.; Duployer, B.; Perez, E. Understanding the Fragmentation Pattern of Marine Plastic Debris. *Environ Sci Technol* **2016,** *50* (11), 5668-5675.
15. Arutchelvi, J.; Sudhakar, M.; Arkatkar, A.; Doble, M.; Bhaduri, S.; Uppara, P. V. Biodegradation of polyethylene and polypropylene. *Indian J Biotechnol* **2008,** *7* (1), 9-22.
16. Andrady, A., Persistence of plastic litter in the oceans. In *Marine anthropogenic litter*, Bergmann, M.; Gutow, L.; Klages, M., Eds. Springer International Publishing: 2015; Vol. Part 1, pp 57-72.
17. Ghaffar, A.; Scott, A.; Scott, G. Chemical and Physical Changes Occurring during Uv Degradation of High Impact Polystyrene. *Eur Polym J* **1975,** *11* (3), 271-275.
18. Craig, I. H.; White, J. R.; Shyichuk, A. V.; Syrotynska, I. Photo-induced scission and crosslinking in LDPE, LLDPE, and HDPE. *Polym. Eng. Sci.* **2005,** *45* (4), 579-587.
19. Perez, C. J.; Failla, M. D.; Carella, J. M. SSA study of early polyethylenes degradation stages. Effects of attack rate, of average branch length, and of backbone polymethylene sequences length distributions. *Polym Degrad Stabil* **2013,** *98* (1), 177-183.
20. Hsu, Y. C.; Weir, M. P.; Truss, R. W.; Garvey, C. J.; Nicholson, T. M.; Halley, P. J. A fundamental study on photo-oxidative degradation of linear low density polyethylene films at embrittlement. *Polymer* **2012,** *53* (12), 2385-2393.
21. Ter Halle, A.; Ladirat, L.; Martignac, M.; Mingotaud, A. F.; Boyron, O.; Perez, E. To what extent are microplastics from the open ocean weathered? *Environ Pollut* **2017,** *227*, 167-174.
22. Gewert, B.; Plassmann, M. M.; MacLeod, M. Pathways for degradation of plastic

polymers floating in the marine environment. *Environmental Science-Processes & Impacts* **2015,** *17* (9), 1513-1521.
23. Jahnke, A.; Arp, H. P. H.; Escher, B. I.; Gewert, B.; Gorokhova, E.; Kuhnel, D.; Ogonowski, M.; Potthoff, A.; Rummel, C.; Schmitt-Jansen, M.; Toorman, E.; MacLeod, M. Reducing Uncertainty and Confronting Ignorance about the Possible Impacts of Weathering Plastic in the Marine Environment. *Environmental Science & Technology Letters* **2017,** *4* (3), 85-90.
24. Bouhroum, R.; Boulkamh, A.; Asia, L.; Lebarillier, S.; Ter Halle, A.; Syakti, A. D.; Doumenq, P.; Malleret, L.; Wong-Wah-chung, P. Concentrations and fingerprints of PAHs and PCBs adsorbed onto marine plastic debris from the Indonesian Cilacap coast and the North Atlantic gyre. *Reg Stud Mar Sci* **2019,** *29*.
25. Prunier, J.; Maurice, L.; Perez, E.; Gigault, J.; Wickmann, A. C. P.; Davranche, M.; ter Halle, A. Trace metals in polyethylene debris from the North Atlantic subtropical gyre. *Environ Pollut* **2019,** *245*, 371-379.
26. Crist, B.; Schultz, J. M. Polymer spherulites: A critical review. *Prog Polym Sci* **2016,** *56*, 1-63.
27. Rouillon, C.; Bussiere, P. O.; Desnoux, E.; Collin, S.; Vial, C.; Therias, S.; Gardette, J. L. Is carbonyl index a quantitative probe to monitor polypropylene photodegradation? *Polym Degrad Stabil* **2016,** *128*, 200-208.
28. Rios, L. M.; Jones, P. R.; Moore, C.; Narayan, U. V. Quantitation of persistent organic pollutants adsorbed on plastic debris from the Northern Pacific Gyre's "eastern garbage patch". *Journal of Environmental Monitoring* **2010,** *12* (12), 2226-2236.
29. Hirai, H.; Takada, H.; Ogata, Y.; Yamashita, R.; Mizukawa, K.; Saha, M.; Kwan, C.; Moore, C.; Gray, H.; Laursen, D.; Zettler, E. R.; Farrington, J. W.; Reddy, C. M.; Peacock, E. E.; Ward, M. W. Organic micropollutants in marine plastics debris from the open ocean and remote and urban beaches. *Mar Pollut Bull* **2011,** *62* (8), 1683-1692.
30. Turner, A.; Solman, K. R. Analysis of the elemental composition of marine litter by field-portable-XRF. *Talanta* **2016,** *159*, 262-271.
31. Dazzi, A.; Prater, C. B.; Hu, Q. C.; Chase, D. B.; Rabolt, J. F.; Marcott, C. AFM-IR: Combining Atomic Force Microscopy and Infrared Spectroscopy for Nanoscale Chemical Characterization. *Appl Spectrosc* **2012,** *66* (12), 1365-1384.
32. Gardette, M.; Perthue, A.; Gardette, J. L.; Janecska, T.; Foldes, E.; Pukanszky, B.; Therias, S. Photo- and thermal-oxidation of polyethylene: Comparison of mechanisms and influence of unsaturation content. *Polym Degrad Stabil* **2013,** *98* (11), 2383-2390.
33. Krimm, S.; Liang, Y.; G., S. Infrared spectra of high polymers. II. polyethylene. *The journal of chemical physics* **1955,** *25* (3), 549.
34. Tobin, M. C.; Carrano, M. J. Infrared spectra of polymers. I. Effect of crystallinity on the infrared spectrum of polyethylene and on the infrared spectra of nylon 6 and nylon 11. *The journal of chemical physics* **1956,** *25* (5), 1044.
35. Guadagno, L.; Naddeo, C.; Vittoria, V.; Camino, G.; Cagnani, C. Chemical and morphologial modifications of irradiated linear low density polyethylene (LLDPE). *Polym Degrad Stabil* **2001,** *72* (1), 175-186.
36. Wunderlich, B. Molecular Nucleation and Segregation. *Faraday Discuss* **1979,** *68*, 239-+.
37. Anwar, M.; Schilling, T. Crystallization of polyethylene: A molecular dynamics simulation study of the nucleation and growth mechanisms. *Polymer* **2015,** *76*, 307-312.
38. Sadler, D. M. New Explanation for Chain Folding in Polymers. *Nature* **1987,** *326* (6109), 174-177.
39. Labana, S.; Labana, L. L. Quinacridones. *Chemical Reviews* **1967,** *67*, 1.

40. Suhrhoff, T. J.; Scholz-Bottcher, B. M. Qualitative impact of salinity, UV radiation and turbulence on leaching of organic plastic additives from four common plastics - A lab experiment. *Mar Pollut Bull* **2016,** *102* (1), 84-94.
41. Cisneros, R. L.; Espinoza, A. G.; Litter, M. I. Photodegradation of an azo dye of the textile industry. *Chemosphere* **2002,** *48* (4), 393-399.
42. Kataoka, H.; Ise, M.; Narimatsu, S. Automated on-line in-tube solid-phase microextraction coupled with high performance liquid chromatography for the analysis of bisphenol A, alkylphenols, and phthalate esters in foods contacted with plastics. *J Sep Sci* **2002,** *25* (1-2), 77-85.
43. Cooper, J. E.; Kendig, E. L.; Belcher, S. M. Assessment of bisphenol A released from reusable plastic, aluminium and stainless steel water bottles. *Chemosphere* **2011,** *85* (6), 943-947.
44. Lin, E. L. C.; Cormier, S. M.; Torsella, J. A. Fish biliary polycyclic aromatic hydrocarbon metabolites estimated by fixed-wavelength fluorescence: Comparison with HPLC-fluorescent detection. *Ecotox Environ Safe* **1996,** *35* (1), 16-23.
45. Nahorniak, M. L.; Booksh, K. S. Excitation-emission matrix fluorescence spectroscopy in conjunction with multiway analysis for PAH detection in complex matrices. *Analyst* **2006,** *131* (12), 1308-1315.
46. Butler, H. T.; Coddens, M. E.; Khatib, S.; Poole, C. F. Determination of Polycyclic Aromatic-Hydrocarbons in Environmental-Samples by High-Performance Thin-Layer Chromatography and Fluorescence Scanning Densitometry. *J Chromatogr Sci* **1985,** *23* (5), 200-207.
47. Hoge, F. E.; Vodacek, A.; Blough, N. V. Inherent Optical-Properties of the Ocean - Retrieval of the Absorption-Coefficient of Chromophoric Dissolved Organic-Matter from Fluorescence Measurements. *Limnol Oceanogr* **1993,** *38* (7), 1394-1402.
48. Fayolle, B.; Richaud, E.; Colin, X.; Verdu, J. Review: degradation-induced embrittlement in semi-crystalline polymers having their amorphous phase in rubbery state. *J Mater Sci* **2008,** *43* (22), 6999-7012.
49. White, J. R.; Turnbull, A. Weathering of Polymers - Mechanisms of Degradation and Stabilization, Testing Strategies and Modeling. *J Mater Sci* **1994,** *29* (3), 584-613.
50. White, J. R. Polymer ageing: physics, chemistry or engineering? Time to reflect. *Cr Chim* **2006,** *9* (11-12), 1396-1408.